iScience

CellPress
OPEN ACCESS

Article

Fast Heat Transport Inside Lithium-Sulfur Batteries Promotes Their Safety and Electrochemical Performance

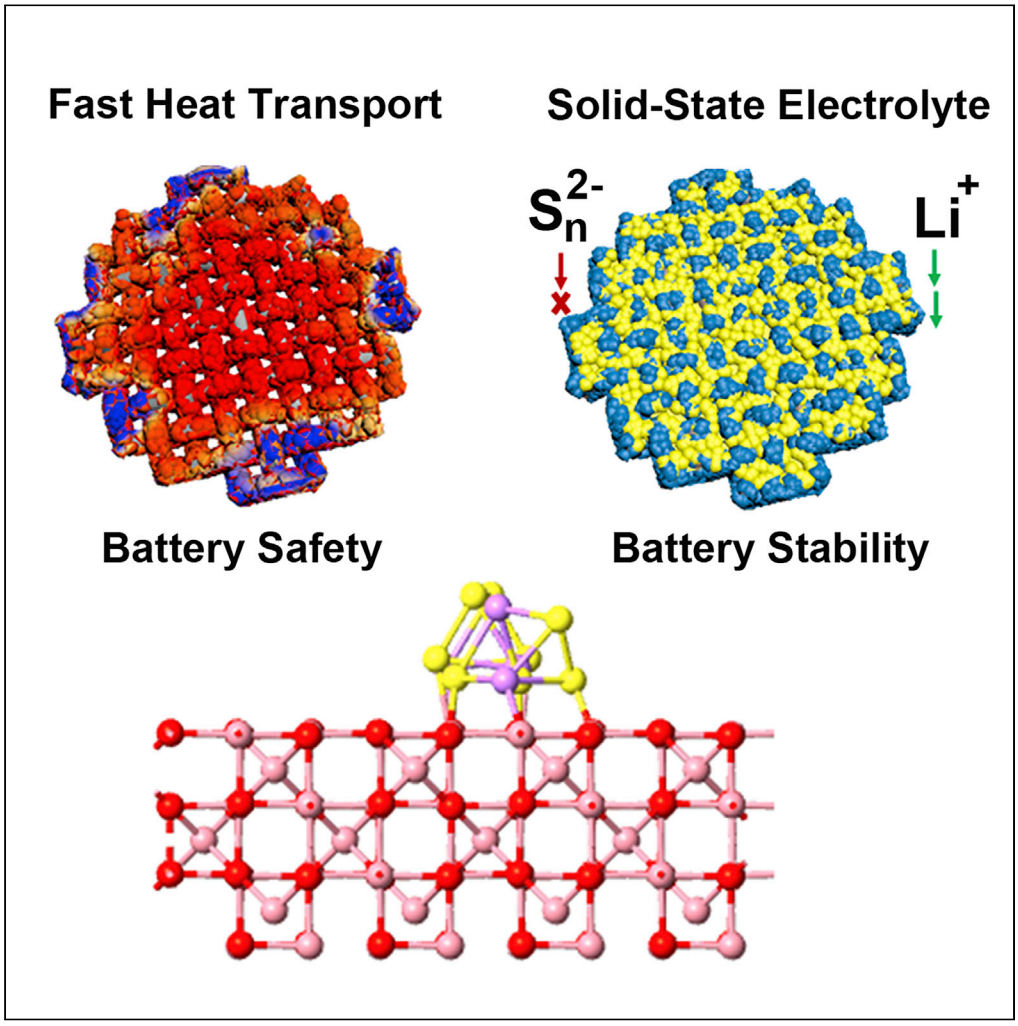

Guiyin Xu, Daiwei Yu, Dongchang Zheng, ..., Mingyuan Ge, Wah-Keat Lee, Meifang Zhu

xuguiyin@mit.edu (G.X.)
zmf@dhu.edu.cn (M.Z.)

HIGHLIGHTS

Fast heat transport inside Li-S batteries was designed by a simple method

Pouch cells showed a good electrochemical performance under a lean electrolyte condition

In situ 2D XANES was conducted to explore the mechanism of Li-S batteries

Xu et al., iScience *23*, 101576
October 23, 2020
https://doi.org/10.1016/j.isci.2020.101576

iScience

CellPress
OPEN ACCESS

Article

Fast Heat Transport Inside Lithium-Sulfur Batteries Promotes Their Safety and Electrochemical Performance

Guiyin Xu,[1,8,*] Daiwei Yu,[2] Dongchang Zheng,[3] Shijian Wang,[4] Weijiang Xue,[1] Xiangkun Elvis Cao,[5] Hongxia Zeng,[3] Xianghui Xiao,[6] Mingyuan Ge,[6] Wah-Keat Lee,[6] and Meifang Zhu[7,*]

SUMMARY

Lithium-sulfur batteries are paid much attention owing to their high specific capacity and energy density. However, their practical applications are impeded by poor electrochemical performance due to the dissolved polysulfides. The concentration of soluble polysulfides has a linear relationship with the internal heat generation. The issue of heat transport inside lithium-sulfur batteries is often overlooked. Here, we designed a functional separator that not only had a high thermal conductivity of 0.65 W m^{-1} K^{-1} but also alleviated the diffusion of dissolved active materials to the lithium anode, improving the electrochemical performance and safety issue. Lithium-sulfur batteries with the functional separator have a specific capacity of 1,126.4 mAh g^{-1} at 0.2 C, and the specific capacity can be remained up to 893.5 mAh g^{-1} after 100 cycles. Pouch Cells with high sulfur loading also showed a good electrochemical performance under a lean electrolyte condition of electrolyte/sulfur (E/S) = 3 μL mg^{-1}.

INTRODUCTION

With the fast development of electric vehicles and unmanned aerial vehicles, energy storage devices with high power and energy density are in urgent need (Xie et al., 2020; Wang et al., 2020). Sulfur has a high specific capacity of 1,675 mAh g^{-1}, which is one of the most promising cathode materials for energy storage devices (Ji et al., 2009). Compared with lithium-ion batteries, lithium-sulfur (Li-S) batteries are based on anion-redox reaction, instead of the lithium intercalation-deintercalation in electrode materials. A common phenomenon in Li-S batteries is the shuttle effect of soluble redox mediators (SRMs, lithium polysulfides in this case) (Mikhaylik and Akridge, 2004), which shuttle between the anode and cathode continuously consuming the electrical energy and thus result in longer charging time than discharging time. The time-dependent heat accumulation would become an issue for both electrochemical performance and safety. On the one hand, the electrolyte additive $LiNO_3$ is very essential to prevent the reactive lithium surface from being corroded by SRMs (Zhang, 2012). There is a minimum concentration of $LiNO_3$ to counteract a fixed concentration of SRMs. If the concentration of SRMs is too high, there would be insufficient $LiNO_3$ to counteract its negative effect. Therefore, the worst case is that the localized heat accumulation can promote the local dissolution of SRMs, which breaks the balance between $LiNO_3$ and SRMs and results in a more severe shuttle effect. On the other hand, from the viewpoint of safety, it is more critical in Li-S batteries than in lithium-ion batteries to avoid the continuous heat accumulation by a good heat transport due to the intrinsic flammability and low boiling temperature of the ether-based electrolyte and possible explosive risk with $LiNO_3$ (similar composition with gunpowder: sulfur, carbon, and KNO_3). Therefore, it clearly calls for an effective approach to transport the heat outward rapidly, which is still absent in previous reports (Zhang, 2012; Zhang et al., 2015; Xu et al., 2017a; Tao et al., 2016; Lin et al., 2017; Fan et al., 2018a; Xue et al., 2020).

To overcome the aforementioned challenges, herein, we prepare a multifunctional separator with a fast heat transport inside Li-S batteries to improve both the safety and the electrochemical performance. The cobalt oxide/carbon composite-modified polypropylene separator has a high thermal conductivity of 0.65 W m^{-1} K^{-1}, which exhibits a fast heat transport during the charged/discharged process. Moreover, the functional separator can chemically trap the dissolved lithium polysulfides and form solid-state electrolyte, stop polysulfides, and transport lithium, further improving their electrochemical performance.

[1]Department of Nuclear Science and Engineering, Massachusetts Institute of Technology, Cambridge, MA 02139, USA

[2]Department of Electrical Engineering and Computer Science, Massachusetts Institute of Technology, Cambridge, MA 02139, USA

[3]Department of Mechanical Engineering, Massachusetts Institute of Technology, Cambridge, MA 02139, USA

[4]Centre for Clean Energy Technology, School of Mathematical and Physical Sciences, University of Technology Sydney, Sydney, NSW 2007, Australia

[5]Sibley School of Mechanical and Aerospace Engineering, Cornell University, Ithaca, NY 14853, USA

[6]National Synchrotron Light Source II, Brookhaven National Laboratory, Upton, NY 11973, USA

[7]State Key Lab for Modification of Chemical Fibers & Polymer Materials, College of Materials Science & Engineering, Donghua University, Shanghai 201620, China

[8]Lead Contact

*Correspondence: xuguiyin@mit.edu (G.X.), zmf@dhu.edu.cn (M.Z.)

https://doi.org/10.1016/j.isci.2020.101576

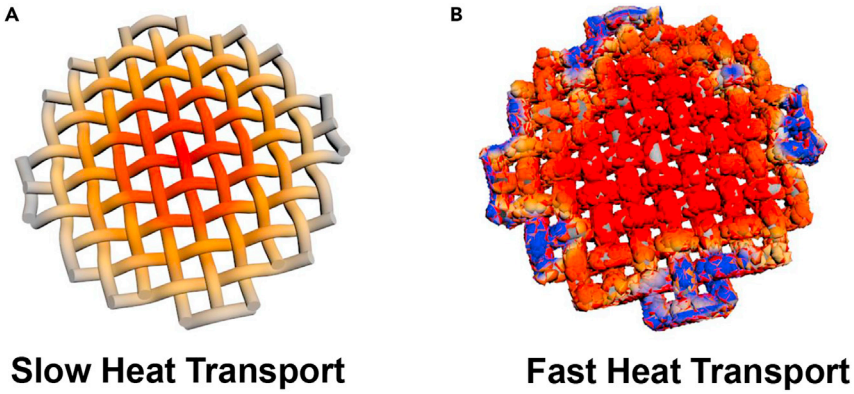

Figure 1. 3D Model Illustration for the Heat Transport of Different Separators
(A and B) (A) Polypropylene separator (PP) and (B) cobalt oxide/carbon composite modified polypropylene separator (CPP).

RESULTS

Heat Transport of CPP

Commercial polymer separators (for example, PP) suffer from low thermal conductivity of ~0.2 W m^{-1} K^{-1} (Yang et al., 2016; Huang et al., 2020), which could not sustain a good heat transport. Thus, the heat is easy to accumulate, inducing the local temperature increase (Figure 1A). Heat highly aggregating in the local part of the separator can facilitate the dissolution of lithium polysulfides, resulting in the poor cycling performance of Li-S batteries. To overcome the difficulty of heat dissipation for PP in the charging/discharging process, a well thermally conductive mixture composed of Co_3O_4, carbon black nanoparticles, and polyvinylidene fluoride (PVDF) binder were coated on PP *via* a simple casting method to construct a heat conductive percolation (Figure 1B). Due to the thermal conductive pathway along the in-plane direction, the designed CPP achieves a higher in-plane thermal conductivity of 0.65 W m^{-1} K^{-1}, which is much higher than that of bare PP and dramatically improves the heat conduction. Thus, a homogeneous thermal distribution of CPP could be ensured during the charging/discharging process, which hinders the locally accelerated dissolution of lithium polysulfides, and thus could enhance the electrochemical performance of Li-S batteries.

The internal heat generation and heat dissipation influence the internal temperature of Li-S batteries (Mikhaylik and Akridge, 2004):

$$P_G = I_C V_H = k_S q_H [S_H] V_H \quad \text{(Equation 1)}$$

$$P_D = \alpha(T - T_0) \quad \text{(Equation 2)}$$

where P_G is internal heat generation power, P_D is heat dissipation power, I_C is charge current, V_H is high plateau voltage, k_s is the shuttle constant, q_H is the specific capacity of the sulfur cathode at the high-voltage plateau during the charging process, and $[S_H]$ is the concentration of SRMs at the high-voltage plateau during the charging process. For the heat dissipation power, α is the overall heat transfer coefficient of Li-S batteries. The internal temperature (T) is close to the ambient temperature (T_0) before Li-S batteries start the high plateau charge. During the charging process, the voltage and heat generation are gradually increased due to the shuttle current and increased concentration of SRMs. The process of increased concentration of SRMs can be expressed as follows:

$$\frac{d[S_H]}{dt} = \frac{I_C}{q_H} - k_S[S_H] \quad \text{(Equation 3)}$$

Equations 4 and 5 represents the change of the internal temperature and steady-state conditions:

$$\frac{dT}{dt} = \frac{1}{mc_h}(P_G - P_D) = \frac{1}{mc_h}\left[k_S q_H [S_H] V_H - \alpha(T - T_0)\right] \quad \text{(Equation 4)}$$

$$P_G = P_D \quad \text{(Equation 5)}$$

where m is the whole mass of Li-S batteries, and c_h is the overall heat capacity of Li-S batteries. When CPP is applied to Li-S batteries, the overall heat transfer coefficient α is increased due to the higher thermal

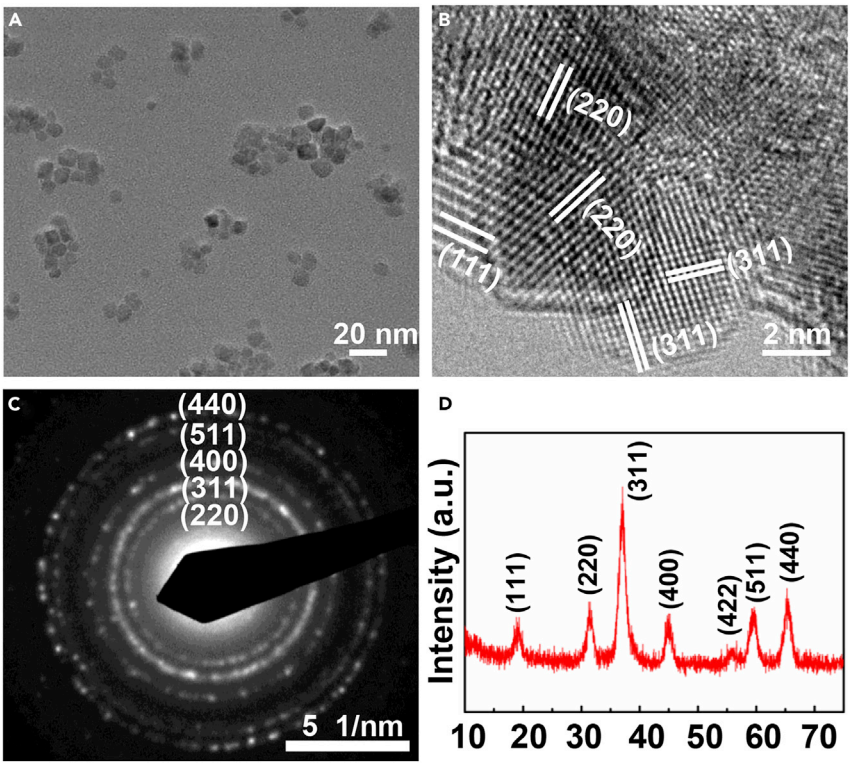

Figure 2. Materials Characterization of Cobalt Oxide

(A–D) (A) Transmission electron microscopy (TEM), (B) high-resolution transmission electron microscopy (HRTEM), (C) selected area electron diffraction (SAED) pattern, and (D) X-ray diffraction (XRD) pattern of cobalt oxide.

conductivity of CPP than that of PP. Thus, P_D is increased. Moreover, $[S_H]$ can be decreased owing to the restriction effect of CCP on the dissolution of SRMs, therefore reducing P_G. The changing rate of internal temperature $\left(dT/dt\right)$ is decreased with the decrease of P_G and increase of P_D. Thus, the internal temperature is lower in the steady-state when CPP is used during the charging process, improving the safety of Li-S batteries.

Characterization of Cobalt Oxide

Cobalt oxide with a particle size of ~5 nm was obtained based on the alcohol-thermal method (Figure 2A) (Dong et al., 2007). Moreover, it is known that metal oxides can become electrically conductive when the particle size is smaller than 10 nm (Xu et al., 2017b). There are abundant crystal surfaces (220, 111, 311) that are exposed in the prepared cobalt oxide for the chemical trap of the dissolved lithium polysulfides (Figure 2B). The selected area electron diffraction (SAED) pattern further confirms the exposed crystal surfaces (220, 311, 400, 511, 440) from cobalt oxide (Figure 2C). XRD results show that the prepared cobalt oxide has good crystallinity with no impurities, and the cobalt oxide has a face-centered cubic phase and is indexed to *JCPDS 09–0418* (Figure 2D).

Characterization of the Cobalt Oxide/Carbon Composite Modified Polypropylene Separator (CPP)

The prepared cobalt oxide was mixed with carbon black and then was coated on the polypropylene separators. The porous structure of CPP is suitable for electrolyte storage and the formation of a solid electrolyte (Figure 3A). The thickness of the polypropylene separator and coating is 25 and 8 um, respectively (Figure 3B). Cobalt, oxygen, and carbon are uniformly distributed on CPP (Figures 3C–3E). Compared with porous polypropylene separators (Figures S1A and S1B), the designed CPP can physically retard the fast diffusion of polysulfides to the anode due to the blocked pores in separators and effectively trap polysulfides by the chemical absorption (Figure 3F) (Xu et al., 2015).

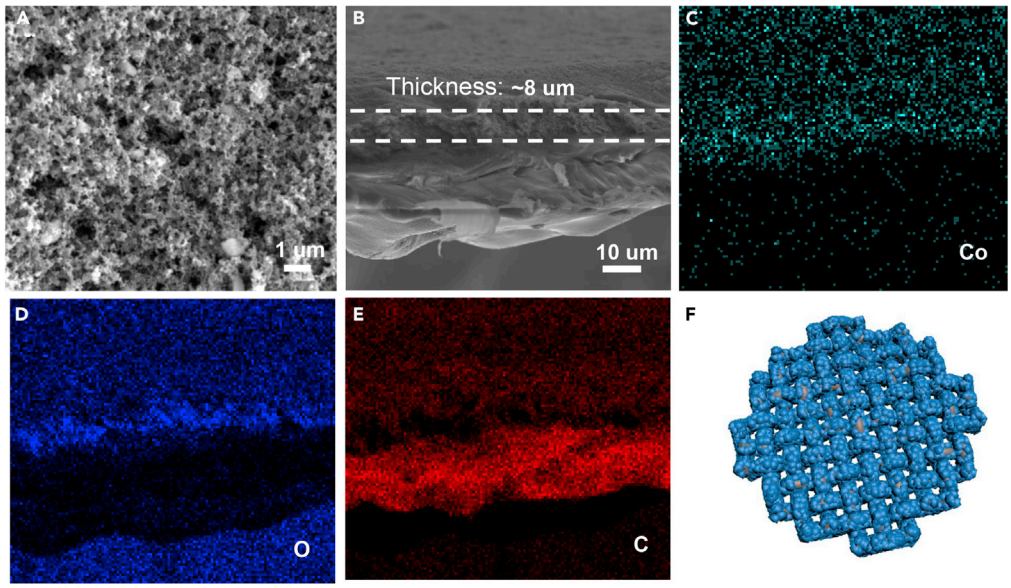

Figure 3. Scanning Electron Microscopy (SEM) and Energy-Dispersive X-ray Spectroscopy (EDS) Characterization of CPP before Cycling

(A–E) (A,B) SEM images of CPP and corresponding elemental mapping images of (C) cobalt, (D) oxygen, and (E) carbon. (F) 3D illustration for the CPP before cycling.

Electrochemical Performance of Li-S Batteries

We assembled coin cells to evaluate the electrochemical performance of Li-S batteries. Firstly, we carried out the CV measurement of sulfur cathode with PP (Figure 4A). There are two reduction peaks at 1.95 and 2.3 V and one oxidation peak at 2.45 V, showing typical electrochemical characteristics of the reduction and oxidation of sulfur (Xu et al., 2019). Then, we checked whether CPP had an electrochemical reaction during the operating voltage range of 1.7–2.8 V (Figure 4B). There is a reduction peak at 2.6 V, corresponding to the lithium embedded into cobalt oxide and thus increasing the ionic conductivity for CPP during the charge/discharge process (Xue et al., 2019). After the first cycle, the CV curves are essentially coincident, indicating the stable electrochemical performance of CPP. Then, we carried out the CV measurement of the sulfur cathode with CPP (Figure 4C). There are two reduction peaks at 2.0 and 2.3 V and one oxidation peak at 2.45 V (Xu et al., 2019). The two reduction peaks correspond to the sulfur reduction reactions, from sulfur to lithium polysulfides (Li_2S_n, $4 \leq n \leq 8$) and further reduction to Li_2S_2/Li_2S. The oxidation peak corresponds to the reaction from Li_2S to lithium polysulfides. The stable oxidation and reduction peaks demonstrate that Li-S batteries with CPP have a good electrochemical performance. The charge/discharge measurement of sulfur cathodes with PP and CPP was tested at the voltage range of 1.7–2.8 V (Figure 4D). There are two apparent discharged plateaus and one charged plateau, which is consistent with the CV results. To compare the electrochemical performance, we assembled coin cells with PP, C-PP, and CPP with a high sulfur loading of 3 mg cm^{-2} (Figure 4E). Li-S batteries with PP have initial specific capacities of 1609.2 and 1213.7 mAh g^{-1} at the current densities of 0.05 C and 0.2 C (1 C = 1675 mA g^{-1}), respectively. Due to the abundant pores in PP, lithium polysulfides are easy to diffuse to lithium anode and thus results in a fast capacity fade. The specific capacity only has 277.4 mAh g^{-1} after 100 cycles. The capacity decay rate is up to 0.8%. The carbon coating polypropylene separators can block the pores on polypropylene and thus physically resist the diffusion of lithium polysulfides to the anode, improving the electrochemical cycling performance. Li-S batteries with C-PP have initial specific capacities of 1390.5 and 1098.8 mAh g^{-1} at the current densities of 0.05 C and 0.2 C, respectively. The specific capacity is 540.8 mAh g^{-1} after 100 cycles. The capacity decay rate is 0.5%. To further reduce the capacity decay rate, we designed the CPP for Li-S batteries. Cobalt oxide and lithium polysulfides can be acted as lewis acid and alkali, respectively; therefore, they have a good chemical cohesion. Moreover, the rich metal sites in cobalt oxide are easy to chemically absorb sulfur in lithium polysulfides due to the metal-sulfur bond formation (Xu et al., 2015). Li-S batteries with CPP have initial specific capacities

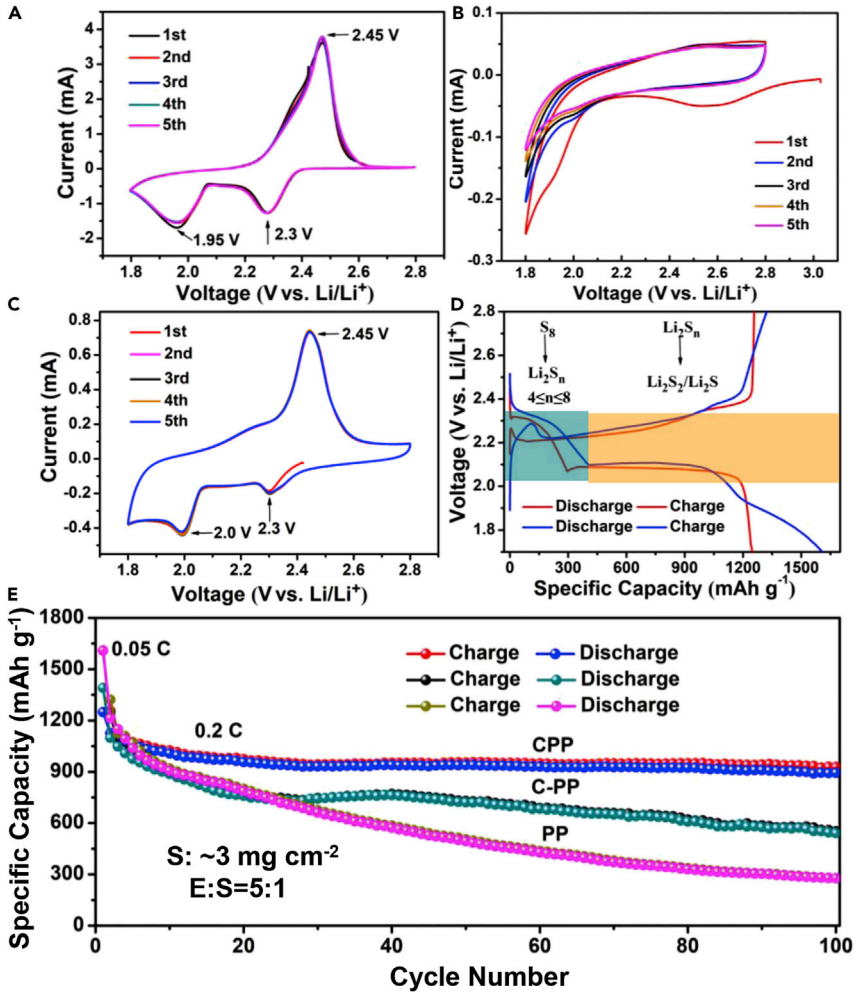

Figure 4. Electrochemical Test of Li-S Batteries by Coin Cells

(A–C) Cyclic voltammetry (CV) curves of (A) PP with sulfur cathodes before cycling, (B) CPP without sulfur cathodes before cycling, and (C) CPP with sulfur cathodes after 100 cycles at 0.2 C.

(D) The charged/discharged curves of sulfur cathodes with PP and CPP.

(E) Cycling performance of sulfur cathodes with different kinds of separators. C-PP: carbon-modified polypropylene separators, PP: polypropylene separators.

of 1248.7 and 1126.4 mAh g^{-1} at the current densities of 0.05 C and 0.2 C, respectively. The specific capacity is 893.5 mAh g^{-1} after 100 cycles. The capacity decay rate is as low as 0.2%, which demonstrates that CPP can improve the electrochemical performance of Li-S batteries. Li-S batteries with CPP have an initial specific capacity of 1435 mAh g^{-1} at 0.1 C and show a good rate performance of 1114.1 mAh g^{-1} at 0.2 C, 1018.0 mAh g^{-1} at 0.5 C, and 998.3 mAh g^{-1} at 1 C (Figure S2). The discharge capacity is still up to 1165.5 mAh g^{-1} when the current density is back to 0.1 C. Moreover, Li-S batteries with CPP have an initial specific capacity of 985.2 mAh g^{-1} at the current density of 1 C (Figure S3). The specific capacity is 857.9 mAh g^{-1} after 100 cycles. The capacity decay rate is as low as 0.1%, which further indicates that CPP can improve the electrochemical performance of Li-S batteries.

We assembled pouch cells to further evaluate the practical performance of Li-S batteries with CPP. The carbon/sulfur cathodes have a dimension of 5.6 cm * 4.3 cm (Figure 5A), and the sulfur loading is up to 5 mg cm^{-2}. The loading of cobalt oxide/carbon composite on PP is 0.8 mg cm^{-2} (Figure 5B). After hand-stacking the cathode, anode, and CPP, Li-S pouch cells were obtained after electrolyte injection and vacuum sealing (Figure 5C). PCCP-based Li-S batteries have initial specific capacities of 860 and 779 mAh g^{-1} at the current

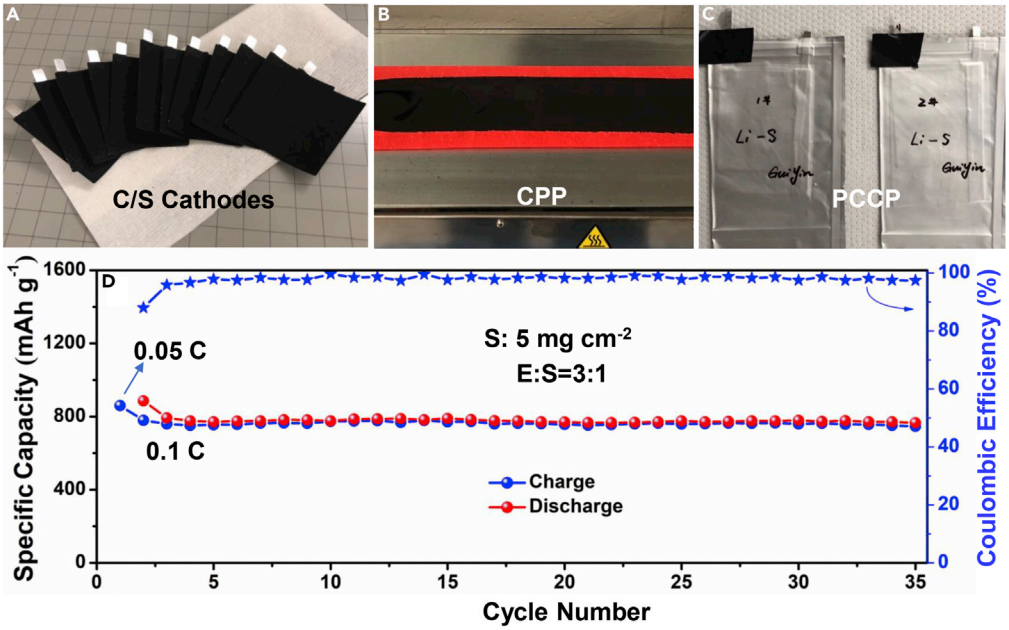

Figure 5. Electrochemical Test of Li-S Batteries by Pouch Cells

(A–D) Digital images of (A) carbon/sulfur (C/S) cathodes with a dimension of 5.6 cm * 4.3 cm, (B) CPP, (C) pouch cells with the cobalt oxide-/carbon-composite-modified polypropylene separator (PCCP). (D) Electrochemical performance of PCCP-based Li-S batteries.

densities of 0.05 C and 0.1 C, respectively (Figure 5D). A high specific capacity of 747 mAh g^{-1} was still achieved after 35 cycles, corresponding to a low capacity decay rate of 0.1% per cycle, and the Coulombic efficiency is up to 99.8%. These excellent electrochemical performances above indicate that CPP is promising for the practical application of Li-S batteries.

DISCUSSION

Functional Mechanism of CPP

The cycled CPP was obtained from cycled Li-S batteries and washed by DOL/DME for several times. The surface of cycled CPP is denser compared with that before cycling (Figure 6A). Cobalt, oxygen, and carbon in the mapping images are from CPP (Figures 6B–6D). The new sulfur mapping image indicates that the CPP effectively intercepts lithium polysulfides (Figure 6E). The solid sulfide electrolyte is formed on the CPP, which can transport lithium but stop polysulfides (Figure 6F) (Xu et al., 2017c), thus further improving the electrochemical performance of Li-S batteries by surface segregation.

The XPS tests of CPP before and after cycling were carried out to analyze the chemical absorption between lithium polysulfides and cobalt oxide. Co^{2+} and Co^{3+} are present in the prepared Co_3O_4 (Figure 7A) (Mi et al., 2019). The peaks at 530.2 and 531.8 eV correspond to the Co-O bond and a hydroxyl group, respectively (Figure 7B) (Zhang et al., 2018). During the discharged process of Li-S batteries, Li_2S_n ($4 \leq n \leq 8$) is easy to dissolve into the organic electrolyte and diffuse to the anode. When Li_2S_n contacts with Co_3O_4, Co^{2+}/Co^{3+} are oxidized to Co^{3+}/Co^{4+}:

$$Li_2S_n\ (4 \leq n \leq 8) + Co^{2+}/Co^{3+} \rightarrow Li_2S_n\ (4 \leq n \leq 8) + Co^{3+}/Co^{4+} \qquad \text{(Equation 6)}$$

The Co 2p XPS spectra of the cycled CPP show the presence of Co^{3+}/Co^{4+} (Figure 7C) (Chen et al., 2016). For the O 1s XPS spectra, the new peak at 533.0 eV can be due to the S-O and Co-O bond (Figure 7D) (Patnaik et al., 2016), and the peak at 531.8 eV corresponds to the Li-O bond (Wood et al., 2018). The new Li-O bond is from the chemical absorption between Li_2S_n and Co_3O_4. In the S 2p XPS spectra (Figure 7E), the peaks could be fitted into eight peaks, corresponding to the S-O (Xu et al., 2015), S-S, Li-S, and S-Co bonds (Fan et al., 2018b). These XPS results demonstrate that CPP can chemically trap the escaped lithium polysulfides by the S-Co, Li-O, and S-O bonds (Figure 7F).

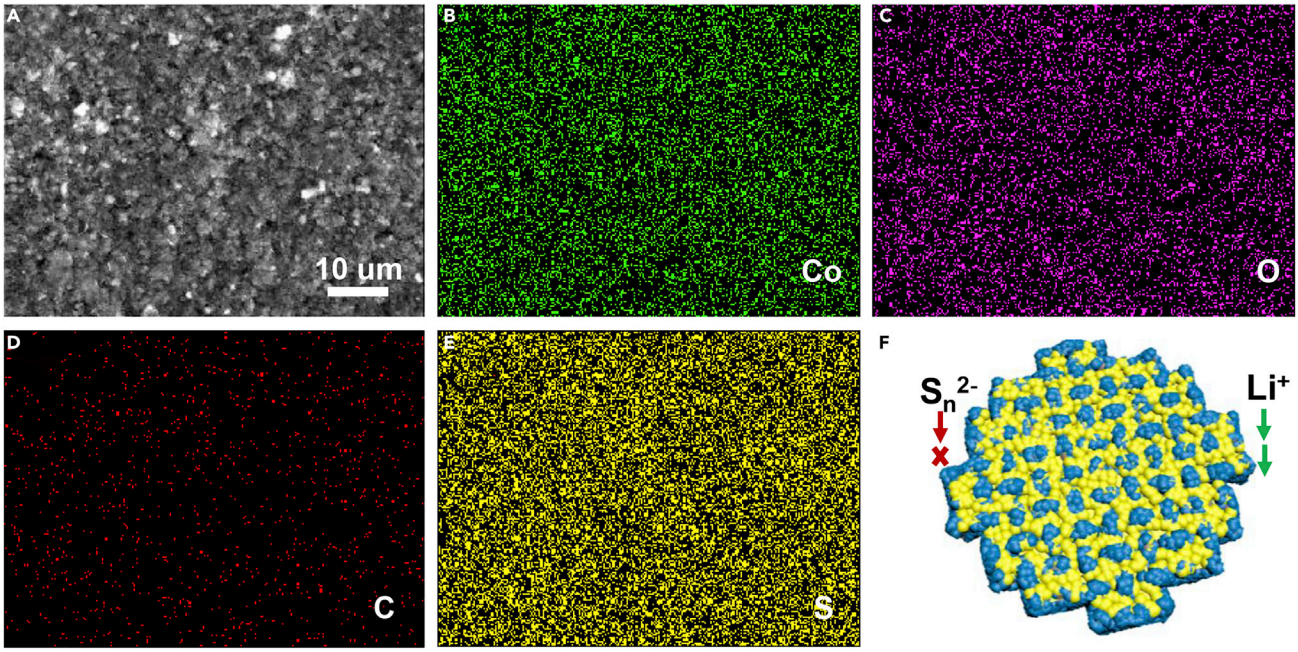

Figure 6. SEM and EDS Characterization of CPP after 100 Cycles at 0.2 C

(A–E) (A) SEM image of CPP and corresponding elemental mapping images of (B) cobalt, (C) oxygen, (D) carbon, and (E) sulfur. (F) 3D illustration for the cycled CPP.

In situ 2D X-ray absorption near-edge spectroscopy (XANES) mapping was performed at FXI beamline (18-ID) at the National Synchrotron Light Source II (NSLS-II), Brookhaven National Laboratory (Figure 8A). Pouch-cell configurations with carbon/sulfur as cathode, lithium metal as anode, and CPP as separator were used for measurements. The pouch cell was firstly discharged to 1.7 V and then charged to 2.8 V at a constant current of 1 mA while collecting XANES spectra. A volume in the middle of the cell was randomly chosen for imaging. 2D XANES images were taken at different energies across the Co absorption edge (7.588–8.153 keV, 1 eV interval). The effective pixel size of each 2D image is 21 nm. Standard samples (Co_3O_4 and $LiCoO_2$) were used to extract the reference absorption spectra for Co^{2+}, Co^{3+}, and Co^{4+} oxidation states. An open-source package PyXAS was used for 2D XANES data analysis (Ge and Lee, 2020). The red and yellow regions correspond to the Co^{3+} and Co^{4+} oxidation states, respectively, further demonstrating the chemical interaction between lithium polysulfides and cobalt oxide, which agrees well with the XPS results and Equation 6.

Conclusion

In conclusion, we successfully prepared a fast heat transport functional separator for Li-S batteries. The electrochemical results of coin cells demonstrated that the cobalt oxide-/carbon-composite-modified polypropylene separators effectively improved the electrochemical performance of Li-S batteries. Importantly, we further assembled pouch cells to evaluate the practical application of Li-S batteries, also showing good electrochemical stability. Moreover, the mechanism analysis was detailly discussed by XPS, XANES, etc., indicating that CPP is promising for Li-S batteries.

Limitations of the Study

In this work, we proposed a multifunctional separator fabricated by a simple coating process. The cobalt oxide/carbon composite modified polypropylene separator has a high thermal conductivity, which has a fast heat transport during the charged/discharged process, improving the electrochemical performance and safety issue. Moreover, the functional separator can chemically trap the dissolved lithium polysulfides and form solid-state electrolytes, stop polysulfides, and transport lithium. However, the thermal conductivity of functional separators should be further increased to obtain an excellent electrochemical performance

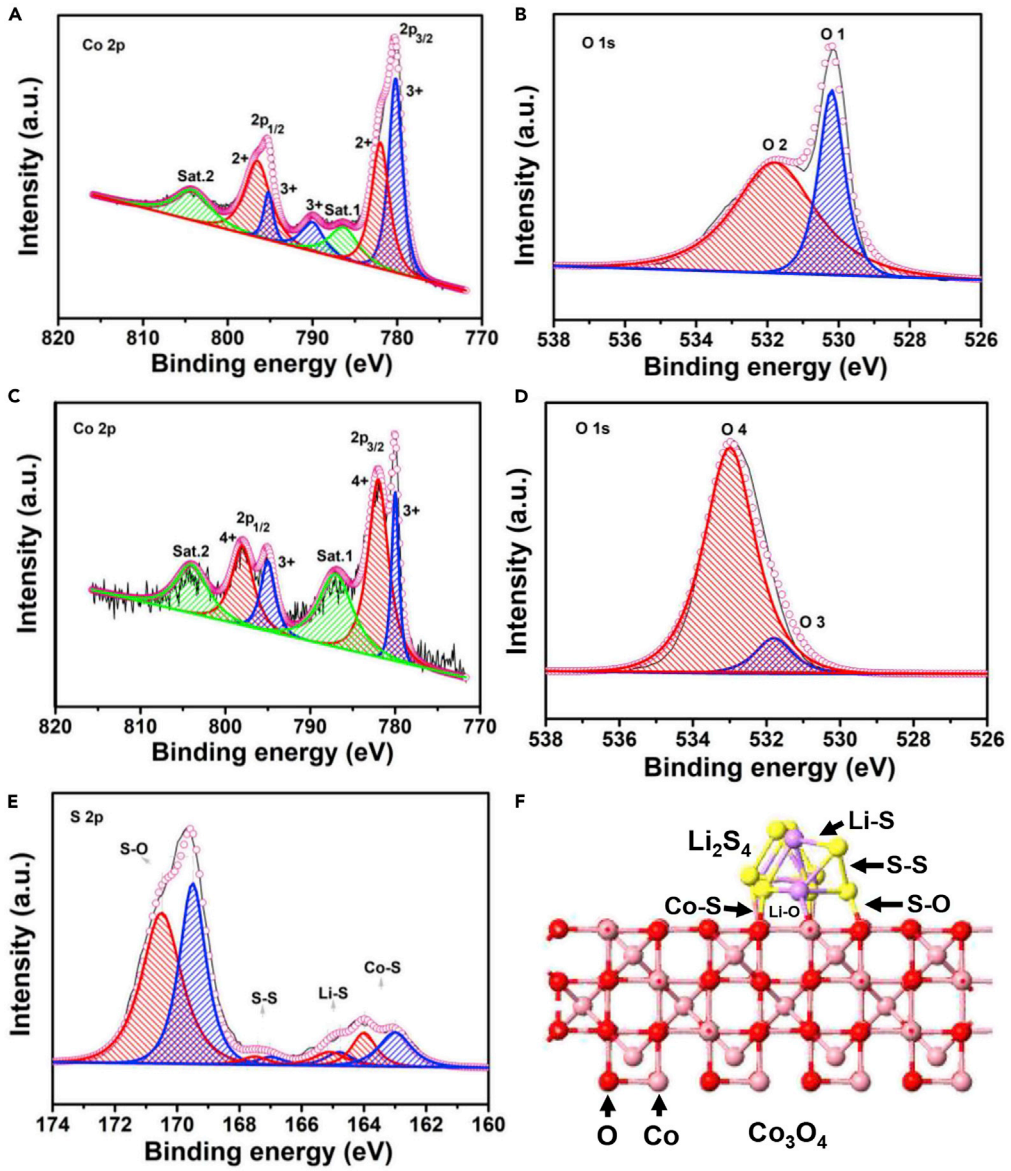

Figure 7. X-ray Photoelectron Spectroscopy (XPS) Spectra of CPP

(A and B) (A) Co 2p and (B) O 1s XPS spectra of CPP before cycling.

(C–F) (C) Co 2p, (D) O 1s, and (E) S 2p XPS spectra of CPP after 100 cycles at 0.2 C. (F) Structure model for the chemical absorption between Li2S4 and Co3O4.

for Li-S batteries. *In situ* characterization (*in situ* XRD, *in situ* Raman, *in situ* SEM, *in situ* SEM, *etc.*) on the interface of functional separators should be explored to further explain the mechanism. *In situ* thermal characterization of pouch cells should be tested to verify the safety issue of Li-S batteries during the charge/discharge process.

Resource Availability

Lead Contact

Further information and requests for resources and reagents should be directed to and will be fulfilled by the Lead Contact, Guiyin Xu (xuguiyin@mit.edu).

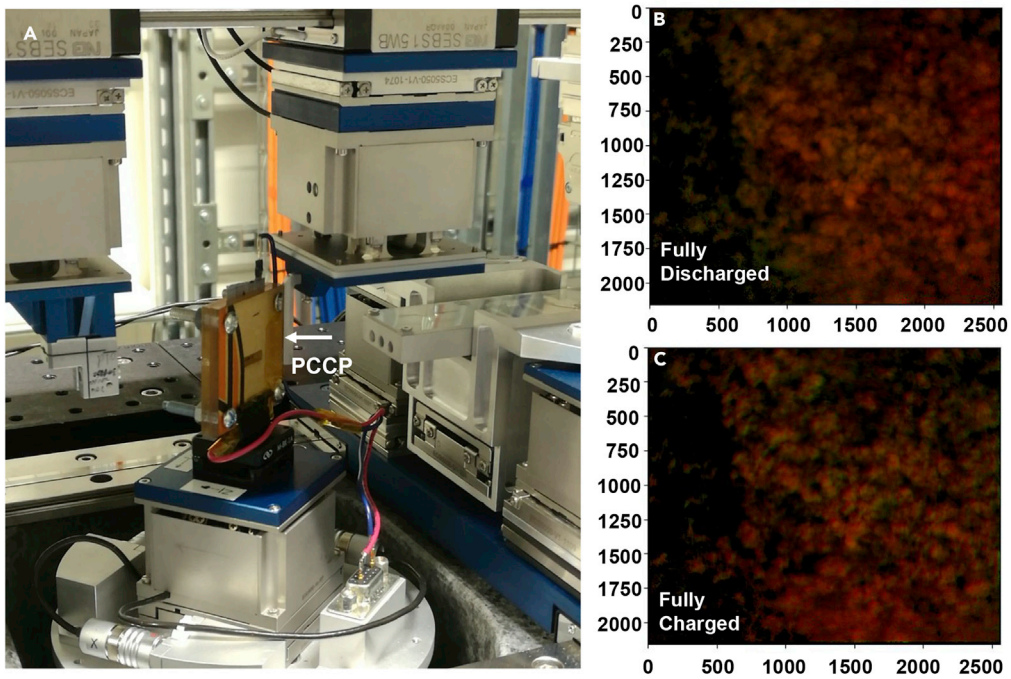

Figure 8. *In Situ* 2D X-ray Absorption Near-Edge Spectroscopy (XANES) Test of Pouch Cell by the Synchrotron-Based Full-Field X-ray Imaging (FXI)

(A–C) (A) Specially designed PCCP for FXI beamline. *In situ* 2D XANES mapping images of Co3O4 particles on CPP at (B) the full discharged state of 1.7 V and (C) the full charged state of 2.8 V.

Materials Availability

This study did not generate new unique reagents.

Data and Code Availability

This study did not generate/analyze datasets/code.

METHODS

All methods can be found in the accompanying Transparent Methods supplemental file.

SUPPLEMENTAL INFORMATION

Supplemental Information can be found online at https://doi.org/10.1016/j.isci.2020.101576.

ACKNOWLEDGMENT

This research used resources of the beamline 18-ID (FXI) of the National Synchrotron Light Source II, a US Department of Energy (DOE) Office of Science User Facility operated for the DOE Office of Science by Brookhaven National Laboratory (DE-SC0012704). M.Z. thanks the support by National Natural Science Foundation of China (51673038).

AUTHOR CONTRIBUTIONS

G. X. and M. Z. conceived the idea. G. X., D. Y., X. X., M. G., and W. L. performed the experiments. G. X. analyzed the results and wrote the paper. All authors discussed the results and contributed to the manuscript.

DECLARATION OF INTERESTS

The authors declare no competing interests.

Received: June 9, 2020
Revised: August 27, 2020
Accepted: September 15, 2020
Published: October 23, 2020

REFERENCES

Chen, Z., Wang, J., Chao, D., Baikie, T., Bai, L., Chen, S., Zhao, Y., Sum, T., Lin, J., and Shen, Z. (2016). Hierarchical porous $LiNi_{1/3}Co_{1/3}Mn_{1/3}O_2$ nano-/micro spherical cathode material: minimized cation mixing and improved Li^+ mobility for enhanced electrochemical performance. Sci. Rep. *6*, 25771.

Dong, Y., He, K., Yin, L., and Zhang, A. (2007). A facile route to controlled synthesis of Co_3O_4 nanoparticles and their environmental catalytic properties. Nanotechnology *18*, 435602.

Fan, X., Ji, X., Han, F., Yue, J., Chen, J., Chen, L., Deng, T., Jiang, J., and Wang, C.S. (2018a). Fluorinated solid electrolyte interphase enables highly reversible solid-state Li metal battery. Sci. Adv. *4*, eaau9245.

Fan, K., Zou, H., Lu, Y., Chen, H., Li, F., Liu, J., Sun, L., Tong, L., Toney, M., Sui, M., et al. (2018b). Direct observation of structural evolution of metal chalcogenide in electrocatalytic water oxidation. ACS Nano *12*, 12369–12379.

Ge, M., and Lee, W.K. (2020). PyXAS – an open-source package for 2D X-ray near-edge spectroscopy analysis. J. Synchrotron Radiat. *27*, 567–575.

Huang, X., Xue, J., Xiao, M., Wang, S., Li, Y., Zhang, S., and Meng, Y. (2020). Comprehensive evaluation of safety performance and failure mechanism analysis for lithium sulfur pouch cells. Energy Storage Mater. *30*, 87–97.

Ji, X., Lee, K.T., and Nazar, L.F. (2009). A highly ordered nanostructured carbon-sulphur cathode for lithium-sulphur batteries. Nat. Mater. *8*, 500–506.

Lin, D., Liu, Y., and Cui, Y. (2017). Reviving the lithium metal anode for high-energy batteries. Nat. Nanotechnol. *12*, 194–206.

Mi, X., Li, Y., Ning, X., Ji, J., Wang, H., Xi, Y., Sun, Y., and Zhan, S. (2019). Electro-Fenton degradation of ciprofloxacin with highly ordered mesoporous $MnCo_2O_4$-CF cathode: enhanced redox capacity and accelerated electron transfer. Chem. Eng. J. *358*, 299–309.

Mikhaylik, Y.V., and Akridge, J.R. (2004). Polysulfide shuttle study in the Li/S battery system. J. Electrochem. Soc. *151*, A1969–A1976.

Patnaik, S., Martha, S., Madras, G., and Parida, K. (2016). The effect of sulfate pre-treatment to improve the deposition of Au-nanoparticles in a gold-modified sulfated g-C3N4 plasmonic photocatalyst towards visible light induced water reduction reaction. Phys. Chem. Chem. Phys. *18*, 28502–28514.

Tao, X., Wang, J., Liu, C., Wang, H., Yao, H., Zheng, G., Seh, Z., Cai, Q., Li, W., Zhou, G., et al. (2016). Balancing surface adsorption and diffusion of lithium-polysulfides on nonconductive oxides for lithium-sulfur battery design. Nat. Commun. *7*, 11203.

Wang, S., Xiong, P., Zhang, J., and Wang, G. (2020). Recent progress on flexible lithium metal batteries: composite lithium metal anodes and solid-state electrolytes. Energy Storage Mater. *29*, 310–331.

Wood, K., Steirer, K., Hafner, S., Ban, C., Santhanagopalan, S., Lee, S., and Teeter, G. (2018). Operando X-ray photoelectron spectroscopy of solid electrolyte interphase formation and evolution in Li_2S-P_2S_5 solid-state electrolytes. Nat. Commun. *9*, 2490.

Xie, X., Liang, S., Gao, J., Guo, S., Guo, J., Wang, C., Xu, G., Wu, X., Chen, G., and Zhou, J. (2020). Manipulating the ion-transfer kinetics and interface stability for high-performance zinc metal anodes. Energy Environ. Sci. *13*, 503–510.

Xu, G., Nie, P., Dou, H., Ding, B., Li, L., and Zhang, X. (2017a). Exploring metal organic frameworks for energy storage in batteries and supercapacitors. Mater. Today *20*, 191–209.

Xu, G., Yan, Q., Wang, S., Kushima, A., Bai, P., Liu, K., Zhang, X., Tang, Z., and Li, J. (2017b). A thin multifunctional coating on a separator improves the cyclability and safety of lithium sulfur batteries. Chem. Sci. *8*, 6619–6625.

Xu, G., Yuan, J., Tao, X., Ding, B., Dou, H., Yan, X., Xiao, Y., and Zhang, X. (2015). Absorption mechanism of carbon-nanotube paper-titanium dioxide as a multifunctional barrier material for lithium-sulfur batteries. Nano Res. *8*, 3066–3074.

Xu, G., Yan, Q., Bai, P., Dou, H., Nie, P., and Zhang, X. (2019). Nano-sized titanium nitride functionalized separator improves cycling performance of lithium sulfur batteries. ChemistrySelect *4*, 698–704.

Xu, G., Kushima, A., Yuan, J., Dou, H., Xue, W., Zhang, X., Yan, X., and Li, J. (2017c). *Ad hoc* solid electrolyte on acidized carbon nanotube paper improves cycle life of lithium-sulfur batteries. Energy Environ. Sci. *10*, 2544–2551.

Xue, W., Shi, Z., Huang, M., Feng, S., Wang, C., Wang, F., Lopez, J., Qiao, B., Xu, G., Zhang, W., et al. (2020). FSI-inspired solvent and "full fluorosulfonyl" electrolyte for 4 V class lithium-metal batteries. Energy Environ. Sci. *13*, 212–220.

Xue, W., Shi, Z., Suo, L., Wang, C., Wang, Z., Wang, H., So, K., Maurano, A., Yu, D., Chen, Y., et al. (2019). Intercalation-conversion hybrid cathodes enabling Li-S full-cell architectures with jointly superior gravimetric and volumetric energy densities. Nat. Energy *4*, 374–382.

Yang, Y., Huang, X., Cao, Z., and Chen, G. (2016). Thermally conductive separator with hierarchical nano/microstructures for improving thermal management of batteries. Nano Energy *22*, 301–309.

Zhang, S.S. (2012). Role of $LiNO_3$ in rechargeable lithium/sulfur battery. Electrochim. Acta *70*, 344–348.

Zhang, S.Y., Li, T.T., Zhu, H.L., and Zheng, Y.Q. (2018). Co_3O_4 polyhedrons with enhanced electric conductivity as efficient water oxidation electrocatalysts in alkaline medium. J. Mater. Sci. *53*, 4323–4333.

Zhang, Q., Cheng, X.B., Huang, J.Q., Peng, H.J., and Wei, F. (2015). Review of carbon materials for advanced lithium-sulfur batteries. Carbon *81*, 850.

iScience, Volume *23*

Supplemental Information

Fast Heat Transport Inside Lithium-Sulfur Batteries Promotes Their Safety and Electrochemical Performance

Guiyin Xu, Daiwei Yu, Dongchang Zheng, Shijian Wang, Weijiang Xue, Xiangkun Elvis Cao, Hongxia Zeng, Xianghui Xiao, Mingyuan Ge, Wah-Keat Lee, and Meifang Zhu

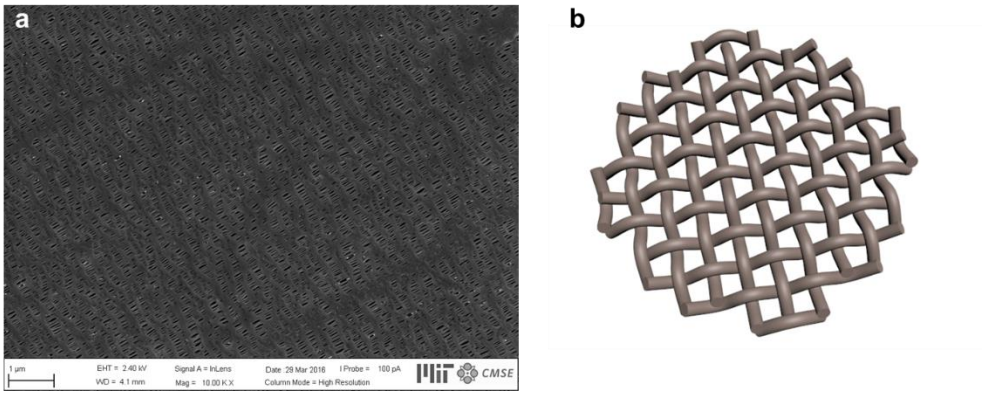

Figure S1. **Materials characterization of PP.** Related to Figure 3. (a) SEM image and (b) 3D illustration of PP.

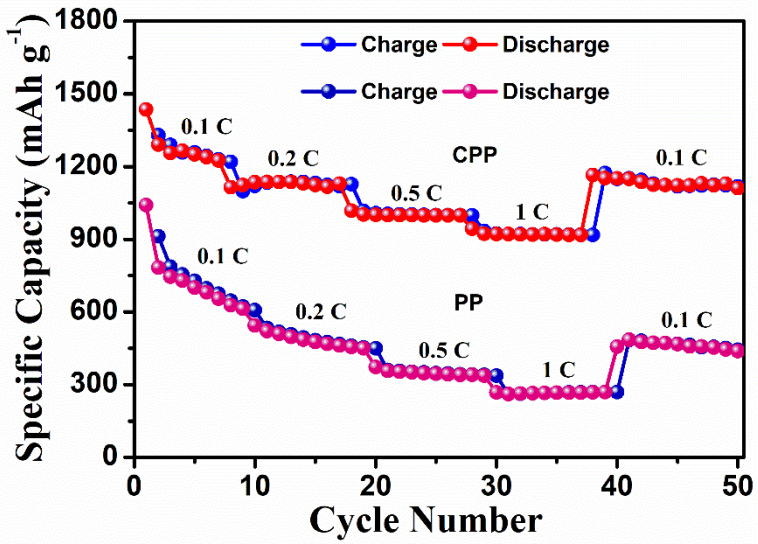

Figure S2. Electrochemical test of Li-S batteries. Related to Figure 4. Rate performance of sulfur cathodes with different kinds of separators.

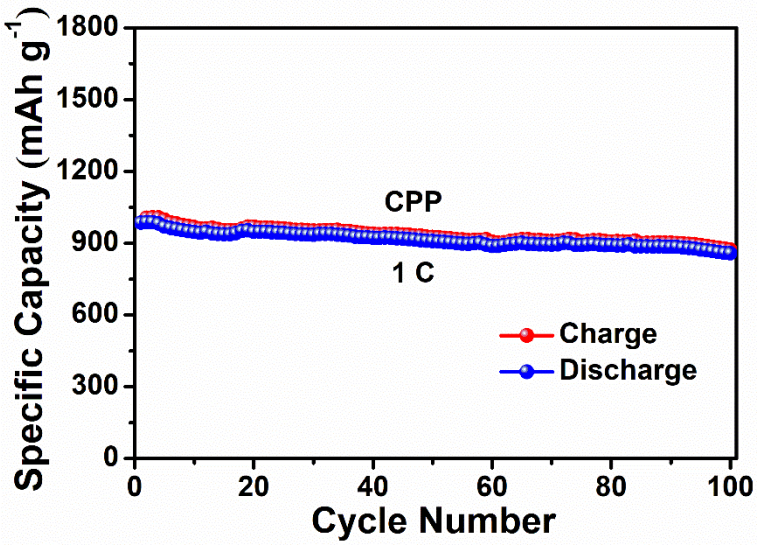

Figure S3. Electrochemical test of Li-S batteries. Related to Figure 4. Cycling performance of sulfur cathodes with CPP at a current density of 1 C.

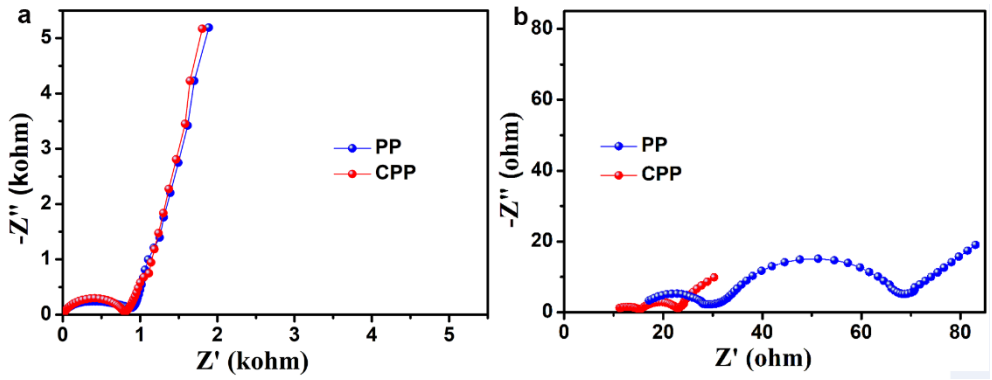

Figure S4. Electrochemical test of Li-S batteries. Related to Figure 4. Impedance plots of sulfur cathodes with PP and CPP (a) before cycling and (b) after 100 cycles at a current density of 1 C.

The impedance plots consist of a semicircle in the high frequency region relating to the interface charge-transfer process (the charge transfer resistance, *Rct*) and a straight line in the low frequency region corresponding to the ion diffusion (the Warburg impedance, W) before cycling. The charge transfer resistance of CPP is smaller than that of PP before cycling (**Figure S4a**). The impedance plots exhibit two depressed semicircles and a sloping line after 100 cycles at a current density of 1 C (**Figure S4b**). The charge transfer resistance of CPP is also smaller than that of PP.

Transparent Methods

Preparation of Cobalt Oxide

1.0 g of cobalt acetate tetrahydrate was dissolved in 50 ml of ethanol and stirred for 30 minutes. 5.0 ml of 25% ammonia was added to the above solution, and then was vigorously stirred for 10 minutes. Then, the obtained homogeneous fuscous slurry was transferred into a 100 ml autoclave. The sealed autoclave was moved into the oven and kept at 150 ℃ for 3 h. The black powder was washed with water and ethanol and dried at 60 ℃ overnight. Finally, cobalt oxide was obtained.

Preparation of the Cobalt Oxide/Carbon Composite Modified Polypropylene Separator (CPP)

CPP was obtained by a slurry coating procedure. The slurry consisted of 70 wt% cobalt oxide, 20 wt% conductive carbon (Super C65), and 10 wt% polyvinylidene fluoride (PVDF) dissolved in N-methyl pyrrolidinone (NMP), and then was uniformly spread on polypropylene separator. And then CPP was dried at 60 °C overnight.

Materials Characterization

Transmission electron microscopy measurement and selected area electron diffraction were carried out with a JOEL 2010F model. X-ray diffraction patterns were measured on a Bruker-AXS D8 DISCOVER. Scanning electron microscopy (SEM) and energy-dispersive X-ray spectroscopy characterization was performed on a Zeiss Merlin high-resolution SEM. X-ray photoelectron spectroscopy analysis was performed on a Perkin-Elmer PHI 550 spectrometer.

Electrochemical Characterization

80 wt% sulfur powder, 12 wt% carbon nanotube, and 8 wt% graphene was mixed as the carbon/sulfur composite. The working electrodes were prepared by a slurry coating procedure. The slurry consisted of 80 wt% carbon/sulfur composite, 12 wt% conductive carbon (Super C65), and 8 wt% LA133 dissolved in water and isopropanol, and then was uniformly spread on aluminum foil current collector. Finally, the electrode was dried at 60 °C overnight. Cells were assembled in an argon-filled glove box using lithium foil as the counter electrode and CPP/polypropylene film as the separator. The

electrolyte was 1 mol L^{-1} LiTFSI and 0.1 mol L^{-1} $LiNO_3$ in a mixed solvent of 1, 3-dioxolane (DOL) and 1, 2-dimethoxyethane (DME) with a volume ratio of 1:1. Coin and pouch cells were galvanostatically charged/discharged between 1.7 and 2.8 V (*vs.* Li/Li^+) using a CT2001A cell test instrument (LAND Electronic Co.). The cyclic voltammetry (CV) measurement was conducted with an electrochemical workstation (Gamry Instruments) at a scan rate of 0.2 mV s^{-1} in the voltage range of 1.8 to 2.8 V (*vs.* Li/Li^+).